Journal of Alloys and Compounds, *188* (1992) 27–35
JALCOM 9004

The crystal chemistry and dielectric properties of the Aurivillius family of complex bismuth oxides with perovskite-like layered structures

B. Frit* and J. P. Mercurio
Laboratoire de Céramiques Nouvelles, U.R.A.-C.N.R.S. No. 320, Faculté des Sciences, Université de Limoges-123, Avenue A. Thomas, 87060 Limoges Cedex (France)

Abstract

Many Aurivillius phases of ferroelectric complex bismuth oxides are currently known. With the formula $Bi_2A_{m-1}B_mO_{3m+3}$, they all consist of Bi_2O_2 layers interleaved with perovskite-like $A_{m-1}B_mO_{3m+1}$ layers. Their crystal chemistry and their chemical stability in relation to the number, m, of octahedral sheets within the perovskite-like layers and to various cationic substitutions, have been analysed. The possibility of their ordered intergrowth, *i.e.* the formation of the homologous series $Bi_4A_{2n-1}B_{2n+1}O_{6n+9}$ of mixed-layer structures has been examined and a comprehensive review of their dielectric properties with respect to various chemical substitutions and to different formation processes has been achieved, permitting an outline of their future potential applications.

1. Introduction

The family of so-called Aurivillius phases [1, 2] is generally formulated as $Bi_2A_{m-1}B_mO_{3m+3}$, or more conveniently $(Bi_2O_2)(A_{m-1}B_mO_{3m+1})$, since the phases are built up by the regular intergrowth of $(Bi_2O_2)^{2+}$ layers and perovskite $(A_{m-1}B_mO_{3m-1})^{2-}$ slabs where A is a combination of cations adequate for 12-coordinated interstices such as Na^+, K^+, Ca^{2+}, Sr^{2+}, Pb^{2+} Ba^{2+}, Ln^{3+}, Bi^{3+}, Y^{3+}, U^{4+}, Th^{4+}, ... etc., B is a combination of cations well suited to octahedral coordination, like Fe^{3+}, Cr^{3+}, Ga^{3+}, Ti^{4+}, Zr^{4+}, Nb^{5+}, Ta^{5+}, Mo^{6+}, W^{6+}, ... etc. and m is an integer which corresponds to the number of two-dimensional sheets of corner-sharing octahedra forming the perovskite-like slabs.

The idealized structures of the first three members of this family ($m = 1$, 2 and 3) are shown as a perspective drawing in Fig. 1 and projected along $[100]_p$ and $[110]_p$ (where the suffix p denotes the cubic perovskite subcell) on Figs. 2 and 3 respectively.

The double-sided Bi_2O_2 sheets are of the kind frequently found in bismuth oxy-compounds, *i.e.* made up of square pyramidal BiO_4 groups sharing their basal edges. All the compounds are tetragonal, or more frequently pseudo-tetragonal (with slight orthorhombic distortion). Their a and b axes lie along $[110]_p$ so that $a \approx b \approx \sqrt{2}a_p \approx 0.54$ nm. Their c axes are inherently long: $c/2 \approx (m + 1)\ 0.413$ nm.

It may be noted that the bismuth atoms of the Bi_2O_2 sheets occupy positions close to virtual A sites, and also that the pyramidal BiO_4 groups share edges in such a way that successive slabs of perovskite structure are in antiphase, displaced by $\frac{1}{2}[110]_p$. Many compounds belonging to this family were synthesized by Smolenskii *et al.* [3] and Subbarao [4, 5]. To date, more than 70 compounds have been reported, including a considerable number of ferroelectrics; some of them are reported in Table 1. They correspond to m values ranging from 1 to 8, but only members of the series for m less than or equal to 5 have now been thoroughly characterized by electron diffraction and high-resolution electron microscopy. The actual existence of the others is therefore doubtful. For example, in the case of the $m = 8$ compounds, $Bi_9Ti_3Fe_5O_{27}$, whose existence was claimed by Ismailzade and co-workers [16, 17], an electron microscope study has shown that it consisted of a mixture of $m = 4$ and $m = 5$ compounds [18].

The aim of this paper is to give an up to date review of the crystallochemical and dielectric characteristics of these fascinating compounds.

2. Crystal chemistry

All these ferroelectric compounds can be described in terms of relatively small amplitude, displacive perturbations away from a high symmetry, prototype, tetragonal parent structure (space group symmetry $I4/mmm$, $a_p = b_p \approx 0.385$ nm), presumed to correspond to the

*Author to whom correspondence should be addressed.

0925-8388/92/$5.00

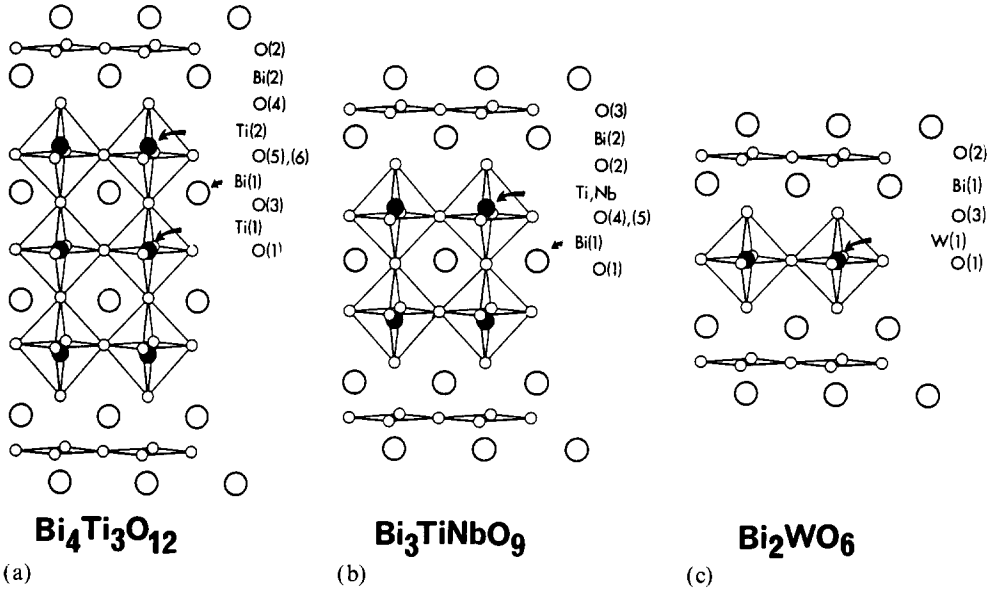

Fig. 1. A perspective drawing of the undistorted *Fmmm* parent structures: (a) $Bi_4Ti_3O_{12}$ ($m = 3$); (b) Bi_3TiNbO_9 ($m = 2$); (c) Bi_2WO_6 ($m = 1$) (from $z \approx 0.25$ to $z = 0.75$).

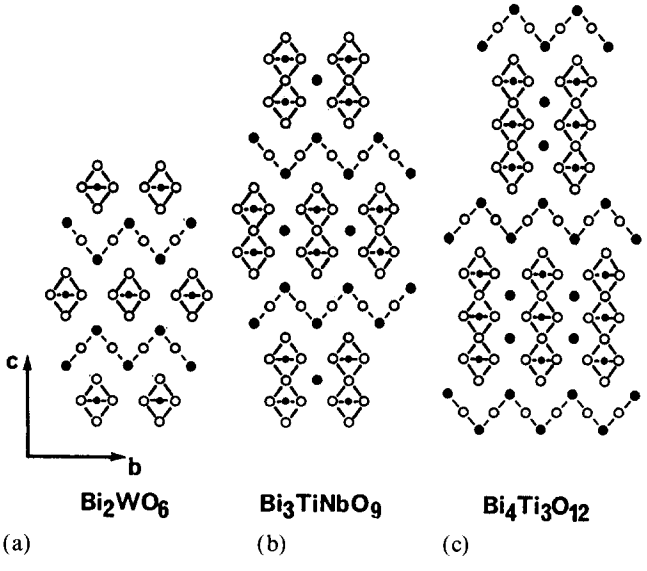

Fig. 2. Idealized structures of: (a) Bi_2WO_6 ($m = 1$); (b) Bi_3TiNbO_9 ($m = 2$); (c) $Bi_4Ti_3O_{12}$. All projected along $[100]_p$.

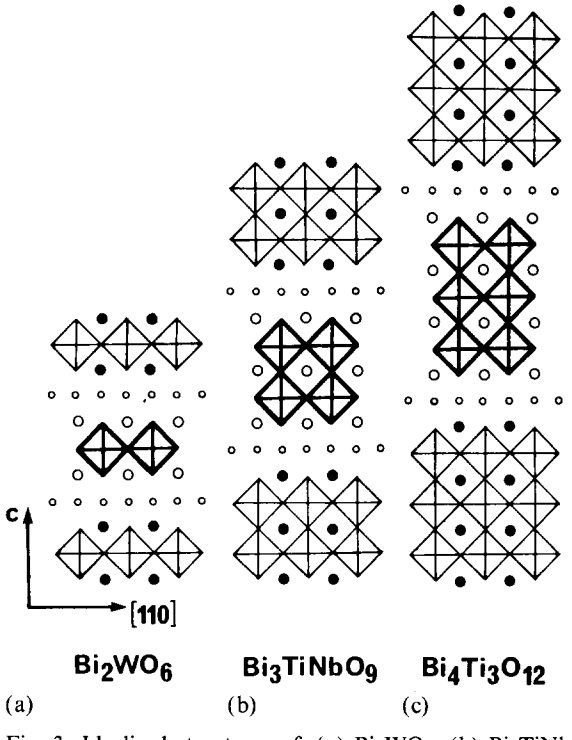

Fig. 3. Idealized structures of: (a) Bi_2WO_6: (b) Bi_3TiNbO_9; (c) $Bi_4Ti_3O_{12}$. All projected along $[110]_p$.

non-polar structure stable above the high temperature ferroelectric–paraelectric phase transition which occurs at their respective Curie temperatures (Figs. 1, 2 and 3). In fact all the known ferroelectric Aurivillius phases have been described on the basis of a doubled orthorhombic (pseudo-tetragonal) diagonal cell ($a = a_p + b_p$, $b = -a_p + b_p$) and of an A-type (for even m) and B-type (for odd m) Bravais lattice, so formally transforming the $I4/mmm$ ($a_p = b_p \approx 0.385$ nm, c) prototype structure to an *Fmmm* ($a \approx b \approx 0.385\sqrt{2}$ nm, c) underlying, non-polar, parent structure. The real structures of Bi_2WO_6 ($m = 1$), Bi_3NbTiO_9 ($m = 2$) and $Bi_4Ti_3O_{12}$ ($m = 3$) as determined by Newnham and co-workers [16, 19, 20] and recently refined by Withers and co-workers [21–23], are shown in Fig. 4.

The deformation from the prototype structure is a direct consequence of an anisotropic behaviour of the lone-pair Bi^{3+} cation. We will analyse it in the case of the Bi_3NbTiO_9 compound [24]. We can see in Fig. 5,

TABLE 1. Examples of reported Aurivillius $Bi_2A_{m-1}B_mO_{3m+3}$ compounds

$m = 1$: Bi_2WO_6 [6], Bi_2MoO_6 [7], Bi_2TeO_6 [8], Bi_2NbO_5F, Bi_2TaO_5F and $Bi_2TiO_4F_2$ [9]
$m = 2$: Bi_3TiNbO_9 [4, 10], $Bi_2PbNb_2O_9$ [4, 5], $Bi_2CaNb_2O_9$ [4, 5], $Bi_{2.5}Na_{0.5}Nb_2O_9$ [1]
$m = 3$: $Bi_4Ti_3O_{12}$ [4], $Bi_2LaTi_3O_{12}$ [11, 12], $Bi_{2.5}Na_{0.5}Nb_3O_{12}$ [13]
$m = 4$: $Bi_4BaTi_4O_{15}$ [4], $Bi_5Ti_3GaO_{15}$ [4], $Bi_5Ti_3FeO_{15}$ [4], $Bi_{4.5}Na_{0.5}Ti_4O_{15}$ [4]
$m = 5$: $Bi_4Pb_2Ti_5O_{18}$ [4], $Bi_5NaNb_4O_{18}$ [1], $Bi_{2.5}Na_{3.5}Nb_5O_{18}$ [13], $Bi_4Pr_2Ti_3Fe_2O_{18}$ [14, 15]
$m = 6$: $Bi_4Pb_3Ti_6O_{21}$ [13]
$m = 7$: $Bi_4Pb_4Ti_7O_{24}$ [13]
$m = 8$: $Bi_9Ti_3Fe_5O_{27}$ [16]

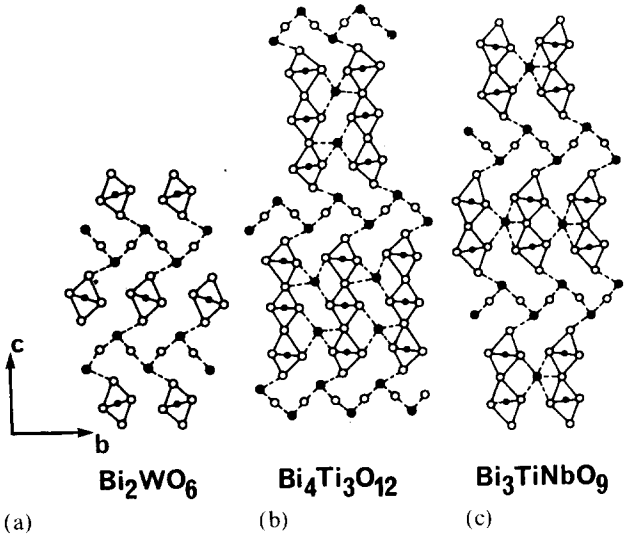

Fig. 4. (011) sections of: (a) Bi_2WO_6; (b) Bi_3TiNbO_9; (c) $Bi_4Ti_3O_{12}$ real structures. Dashed lines indicate strong Bi–O bonds.

where short Bi–O distances are visualized, that two kinds of atomic movements are observed:

(i) Atomic movements parallel to (001) (Fig. 5(a)): the Nb,Ti atoms are shifted along the polar axis a away from the centre of the octahedra and the octahedra rotate about c. This leads to a global decrease of the a and b parameters and to a slight orthorhombic distortion ($b < a$).

(ii) Atomic movements parallel to (100) (Fig. 5(b)). Because of the very short Bi(1)–O(1) distance, the first is the rotation of the (Nb,Ti)O_6 octahedra around a. This rotation is enhanced by the fifth strong bond Bi(2)–O(2) contracted by the Bi(2) atom of the (Bi_2O_2) layers with one of the apex O(2) atoms of the perovskite layer, in addition to the four Bi(2)–O(3) bonds of the square pyramid configuration. The corresponding (Nb,Ti)–O(1) distance increases strongly. This results in a strong elongation of the octahedra along c and, despite tilting around a, in an increase of the thickness of the perovskite layer, *i.e.* of the c parameter.

In conclusion, the distortions caused by the asymmetric Bi^{3+} cations result in an increase of the c parameter and a decrease of both a and b parameters, together with an orthorhombic distortion.

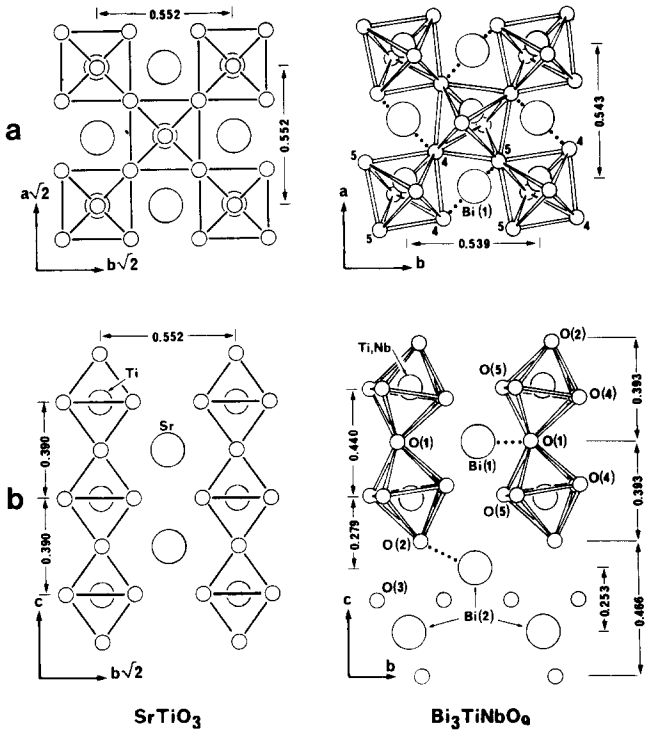

Fig. 5. Comparison of the distorted perovskite layers of the Bi_3TiNbO_9 structure with an ideal cubic layer ($SrTiO_3$). The very short Bi(1)–O(1) distance and the fifth strong Bi(2)–O(2) bond are indicated by dotted lines.

The replacement of the asymmetric Bi^{3+} cations by symmetric La^{3+} cations should logically cancel the distortions, and therefore should result in the opposite evolution: this is actually observed with the $Bi_{3-x}La_xTiNbO_9$ solid solution ($0 \leqslant x \leqslant 1$) where the evolution of the unit cell parameters and their composition is shown in Fig. 6. Such a phenomenon is logically not observed when the octahedral cations Nb^{5+} are replaced by Ti^{4+} and W^{6+} cations, as in the $Bi_3Ti_{1+x/2}Nb_{1-x}W_{x/2}O_9$ solid solution ($0 \leqslant x \leqslant 1$) (Fig. 7).

2.1. Stability

As in pure perovskite structures, it is the relative size of cations A and B which determines, via the classical tolerance factor $t = (r_A + 0.140)/\sqrt{2}(r_B + 0.140)$, the stability of the structure. The possibilities are, however, reduced because of the necessity for adjacent Bi_2O_2 and

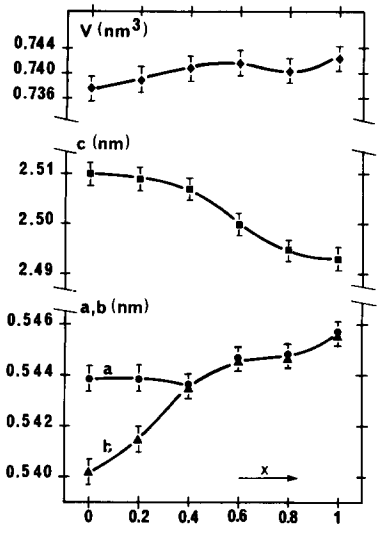

Fig. 6. $Bi_{3-x}La_xTiNbO_9$: evolution of the lattice parameters with x.

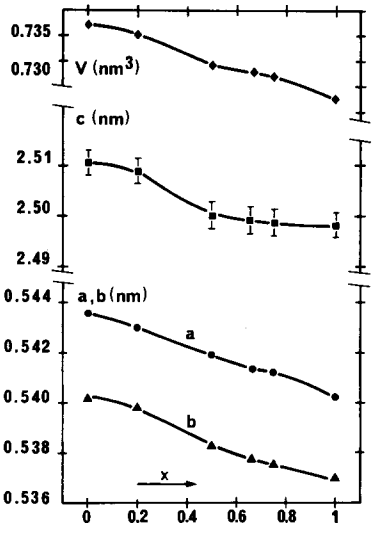

Fig. 7. $Bi_3Ti_{1+x/2}Nb_{1-x}W_{x/2}O_9$: evolution of the lattice parameters with x.

perovskite layers to conform to the same lateral dimensions.

In fact, Subbarao [4] noticed that the tolerance factors for the perovskite layer were in the range 0.81–0.93, *i.e.* had a narrower range than that observed for perovskites (0.77–1.01). Similarly, Ismailzade and coworkers [16, 25] calculated the tolerance factors and concluded that a layer structure may be formed if $0.87 < t < 0.99$. By examining the solubility limit of various cations in A and B sites of $Bi_4Ti_3O_{12}$ Armstrong and Newnham [26] noticed that:

(i) The lattice parameter, a, for $Bi_4Ti_3O_{12}$ (0.383 nm) is approximately halfway between the estimated lattice parameter of the unconstrained $Bi_2Ti_3O_{10}$ perovskite layer (0.389 nm) and that of the unconstrained Bi_2O_2 layer (0.380 nm).

(ii) The bismuth atoms in the perovskite layer can be replaced by atoms with ionic radii between 0.134 nm (Ca^{2+} in 12-coordination) and 0.161 nm (Ba^{2+}) and cations in the range 0.059 (W^{6+}) to 0.065 (Fe^{3+}) nm can substitute for Ti^{4+} in the octahedral site. It must be noted that the octahedral site in pure oxide perovskites accepts cations ranging in size from 0.0535 (Al^{3+}) to 0.087 (Ce^{4+}) nm.

(iii) In both cases, the lower limit of the ionic radii is determined by the stability of the perovskite layer and the upper limit by the mismatch between the Bi_2O_2 and perovskite layers.

The pyramidal coordination of bismuth atoms within the Bi_2O_2 layers is unattractive to symmetric cations and potential candidates are therefore limited to Pb^{2+} and La^{3+} which form similar pyramidal Pb_2O_2 and La_2O_2 layers in the red PbO polymorph and La_2MoO_6 respectively. However, if La^{3+} cations actually substitute partially for Bi^{3+} cations of the $(Bi_2O_2)^{2+}$, since in the $Bi_{4-x}La_xTi_3O_{12}$ solid solution the upper x limit is 2.8 according to Armstrong and Newnham [26] and even 3 according to Ismailzade and Mirishli [17], and since a solid solution $Bi_{2-x}La_xWO_6$ has been observed by Watanabe *et al.* [27] for $0 \leqslant x \leqslant 1.1$, on the contrary Pb^{2+} substitution seems limited to the A site of the perovskite layers and the lead analogues to bismuth titanate are not observed. The absence of interlayer bonding may be the reason. A Pb_2O_2 layer would be electrostatically neutral, reducing the attractive forces between layers.

As far as anionic substitution is concerned, and contrary to what might have been supposed, considering the early synthesis by Aurivillius [9] of the layered oxyfluorides Bi_2NbO_5F, Bi_2TaO_5F ($m = 1$) and $Bi_2TiO_4F_2$ ($m = 2$), the substitution of fluorine for oxygen according to $Bi_2A_{m-1}B_mO_{3m+3-n}F_n$ is very difficult to realize since the only oxyfluorides so far isolated with certainty are $Bi_3Ti_2O_8F$ ($m = 2, n = 1$), $PbBi_3Ti_3O_{11}F$ ($m = 3, n = 1$) [28], $Bi_2PbTiTaO_8F$, $Bi_2PbTiNbO_8F$ ($m = 2, n = 1$), $Bi_5Ti_2WO_{14}F$ and $Bi_7Ti_5O_{20}F$ [29]. The last two compounds are members of a new family of mixed-layered bismuth compounds which will be described in a following chapter.

2.2. *High values of m*

Theoretically, all the values from $m = 1$ to $m = \infty$ (pure perovskite) are possible in so far as the geometrical rules of ion packing are respected within the perovskite layers and the elastic strains induced by the connection of the different two layers are acceptable. Only a few systems have been systematically investigated in order to try to synthesize high-order superstructures: they correspond to various mixtures:

$Na_{0.5}Bi_{2.5}Nb_2O_9$–$n NaNbO_3$,

i.e. $Bi_{2.5}Na_{m-1.5}Nb_mO_{3m+3}$

$Bi_4Ti_3O_{12}$–$n PbTiO_3$,

i.e. $Bi_4Pb_{m-3}Ti_mO_{3m+3}$ [13]

$Bi_4Ti_3O_{12}$–$n BiFeO_3$,

i.e. $Bi_4Bi_{m-3}Ti_3Fe_{m-3}O_{3m+3}$ [17]

$Bi_2CaNb_2O_9$–$n NaNbO_3$,

i.e. $Bi_2CaNa_{m-2}Nb_mO_{3m+3}$ [30, 31]

The results are often confusing and contradictory, which is not surprising if one considers the difficulty in unambiguously characterizing such phases and accurately indexing powder X-ray diffraction patterns. Nevertheless, it clearly appears that phases with $m > 5$ are very difficult to synthesize and order. Kikuchi and co-workers' [32] efforts to prepare members with $m > 7$ in the lead system and $m > 5$ in the sodium system were unsuccessful. They justified these results on the basis of an elastic model which showed that, in such a system, increasing m results in an increase in the lateral dimensions of the perovskite layers and therefore in the layer mismatch.

Horiuchi and co-workers [30, 31] have shown that in the sample with the nominal composition $Bi_2CaNb_2O_9$–$8NaNbO_3$, the phases with $m = 6$–8 appear predominantly. However, all these phases grow only in limited regions in which different values of m intergrow very finely and in a disordered way (see lattice images of Fig. 8). An increase in the annealing time during synthesis does not result in a substantial change in the structure. This presumably suggests that the minima in the free energy curves of these phases are almost equal.

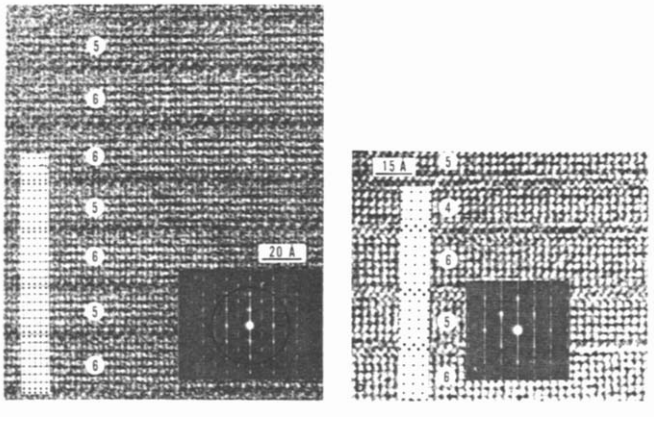

Fig. 8. 1 MV high-resolution electron microscope images of the $Bi_2CaNa_{m-2}Nb_mO_{3m+3}$ phases showing the disordered intergrowth of phases mainly with $m = 5$ and 6. The incident beam is normal to the (100) and (110) planes for (a) and (b) respectively (from Horiuchi and co-workers [29, 30]).

2.3. *Mixed-layered structures*

The frequent occurrence of microsyntactic (disordered) intergrowths suggests the possibility of formation, in selected systems and with a favourable thermal treatment, of recurrent (ordered) intergrowths. It is effectively tempting to imagine a new family of mixed-layer type bismuth compounds whose structure would be built up by a regular intergrowth of one half the unit cell of an m member superstructure and one half the unit cell of an $(m + 1)$ member superstructure along c. They would have the formula

$$(Bi_2O_2)(A_{m-1}B_mO_{3m+1}) + (Bi_2O_2)A_{m'-1}B_{m'}O_{3m'+1}),$$

i.e. $Bi_4A_{m+m'-2}B_{m+m'}O_{3(m+m')+6}$

or, if we suppose that only m and $(m + 1)$ members can be intergrown,

$$Bi_4A_{2n-1}B_{2n+1}O_{6n+9}$$

The ideal structures of the first three members of this new homologous series are shown in Fig. 9.

In fact, various ordered intergrowths have been recently observed and isolated as macroscopic pure phases. They are reported in Table 2.

The a and b parameters have values in the range 0.541–0.547 and 0.544–0.547 nm and the c parameter

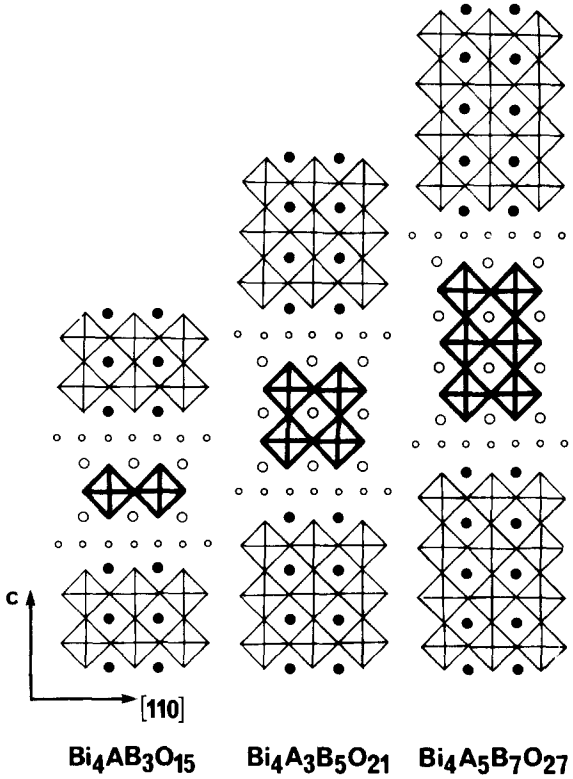

Fig. 9. Schematic illustration of the first three members of a homologous series of mixed layer structures with general formula $Bi_4A_{2n-1}B_{2n+1}O_{6n+9}$.

TABLE 2. Known $Bi_4A_{2n-1}B_{2n+1}O_{6n+9}$ mixed-layer compounds

Intergrowth	Compounds	References
$n = 1$ (1 + 2)	$Bi_5TiNbWO_{15}$	32
	$Bi_5Nb_3O_{15}$	33
	$Bi_{4.5}Na_{0.5}Nb_2WO_{15}$	32
	$Bi_5Ti_{1.5}W_{1.5}O_{15}$	34
$n = 2$ (2 + 3)	$Bi_7Ti_4NbO_{21}$	32, 35
	$Bi_7Ti_4TaO_{21}$	32
	$Bi_6SrTi_3Nb_2O_{21}$	32
	$Bi_6BaTi_3Nb_2O_{21}$	32
	$Bi_7Ti_{4.5}W_{0.5}O_{21}$	33
$n = 3$ (3 + 4)	$Bi_8SrTi_7O_{27}$	32, 36
	$Bi_8BaTi_7O_{27}$	32, 33, 34, 38
	$Bi_8PbTi_7O_{27}$	32
	$Bi_{8.5}Na_{0.5}Ti_7O_{27}$	32
	$Bi_9Ti_6CrO_{27}$	33, 34, 37, 38

is almost one-half of the sum of the c values of the respective members intergrown. Their structures have been confirmed by high-resolution electron microscopy and in some cases refined by matching the experimental and computer-simulated images (see Figs. 10 and 11). However, they are not easily prepared and if elastic interactions alone seem to be responsible for the long periodicity [33] their stability is still the subject of much speculation.

2.4. Dielectric properties

As mentioned above, the majority of the Aurivillius phases are orthorhombic and ferroelectric at room temperature, with polar axes parallel to a.

Recent refinement of the crystal structures of Bi_2WO_6 [23], Bi_3TiNbO_9 [21] and $Bi_4Ti_3O_{12}$ [22] have clearly shown that the octahedral shape of the oxygen framework in the perovskite slabs of the parent structure

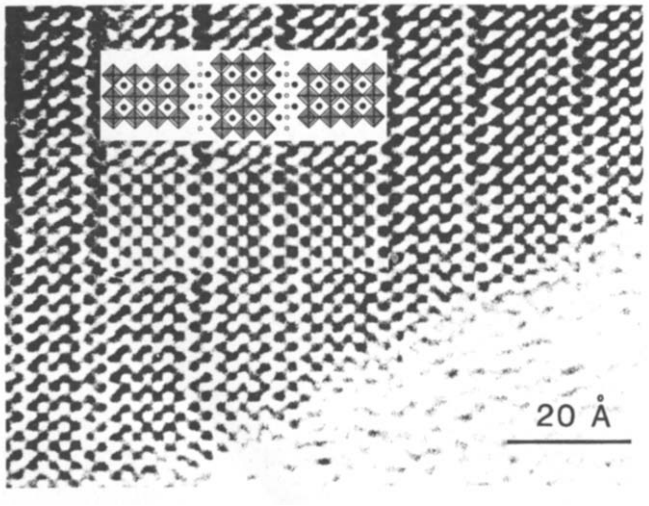

Fig. 10. High-resolution image of $Bi_9Ti_6CrO_{27}$ recorded at 500 kV (after Gopalakrishnan *et al.* [33]).

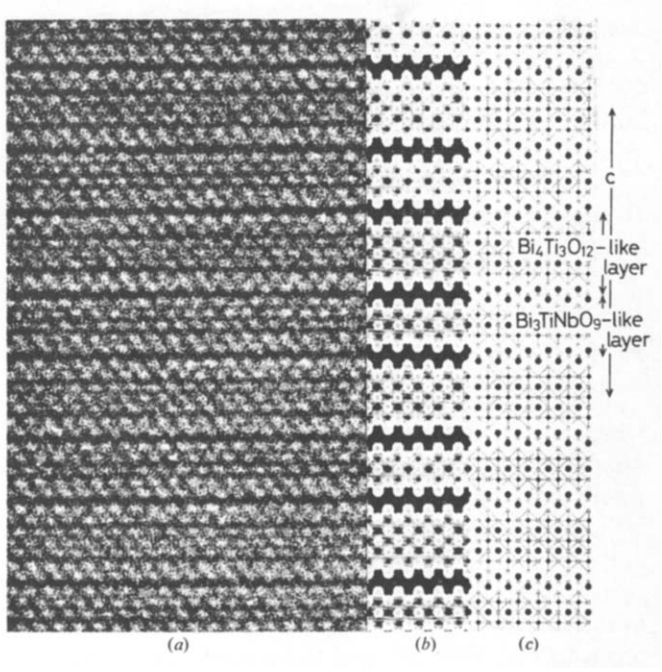

Fig. 11. High-resolution image of $Bi_7Ti_4NbO_{21}$ taken at 1000 kV (a); simulated image (b); model structure viewed along [110] (c) (after Horiuchi *et al.* [35]).

remains nearly intact and that the main structural cause of ferroelectricity in these three compounds is the a axis displacement of Bi atoms in the perovskite A sites with respect to the chains of TiO_6 octahedra and not, as previously believed [12], the perovskite B atoms moving towards an octahedral edge (see Table 3).

However, in the case of $Bi_4Ti_3O_{12}$ whose symmetry changes from tetragonal to monoclinic below the Curie temperature, there is a small component of this polarization along the c axis: single crystals show hysteresis loops with saturation polarization of 0.3–0.5 C m^{-2} along the a-axis and 0.04 C m^{-2} along the c axis [40].

The room temperature dielectric permittivities range between 100 and 200, with dielectric losses less than 1%. The Curie temperatures, as well as the nature of the

TABLE 3. The relative contribution to the calculated spontaneous polarization (C m^2) of the three types of *F2mm* motion along the a direction (after Withers *et al.* [39])

Compound	Oct.[a]	B[b]	Ot[c]
$Bi_4Ti_3O_{12}$	0.221	0.117	0.032
Bi_3TiNbO_9	0.147	0.097	0.025
Bi_2WO_6	0.114	0.251	0.097

[a]The contribution due to the averaged shift along a of the B_nO_{3n+1} part of the perovskite slabs. [b]The contribution due to the averaged motion back in the opposite direction of the perovskite B cation with respect to its surrounding oxygen octahedral framework. [c]The contribution due to the averaged motion along the a direction of the oxygen ions within the Bi_2O_2 layer.

associated phase transition, change with both the number m of perovskite layers and the nature of the octahedral and/or the cubooctahedral cations. Systematic trends are difficult to draw from these evolutions, except perhaps that, as shown in Fig. 12, for given m and octahedral cations, the smaller the ionic radius of the cubooctahedral cation the higher the corresponding Curie temperature [41]. However, the dielectric properties of these interesting materials can be modulated and tailored in several ways as, *e.g.* in chemical substitutions or anisotropic ceramic processing.

During the last thirty years many substitutions involving both octahedral and cubooctahedral cations have been performed. The most spectacular changes are observed when lanthanoid cations are substituted for Bi^{3+} in the cubooctahedral cavities: the Curie temperature strongly decreases and the ferro–paraelectric transition becomes more diffuse than in the unmodified phase (see, *e.g.* the case of La-substituted Bi_3TiNbO_9 [24] in Fig. 13). The influence of octahedral substitution is logically less important, since the cations involved (Ti^{4+}, Nb^{5+}, W^{6+}) are not very different in size and do not play a major structural role in the polarization process. As a consequence the transition remains sharp (Fig. 14). In the case of a mixed substitution (*e.g.* $Bi^{3+} + Ti^{4+} \rightarrow M^{2+} + Nb^{5+}$) the Curie temperature decreases with the decreasing Bi content [5, 42].

By comparison with barium titanate ($BaTiO_3$) or lead zirconate titanate (PZT) ceramics, the bismuth layer compounds are characterized by: (i) lower dielectric constants; (ii) higher Curie temperatures; (iii) lower temperature coefficients of the resonant frequency; (iv) stronger anisotropic electromechanical coupling factors; (v) a lower ageing rate (Table 4). Thus, such materials

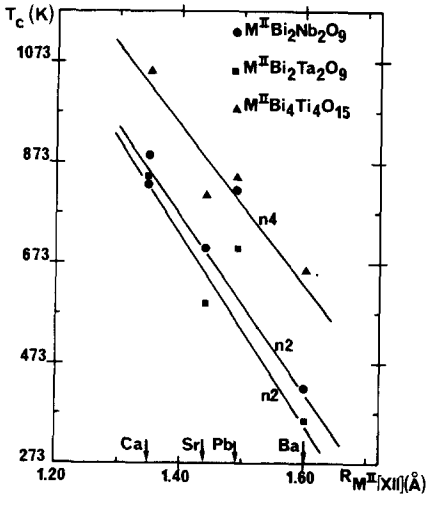

Fig. 12. Evolution of the Curie temperature of some bismuth layered compounds with the ionic radius of the cubooctahedral M^{II} cations.

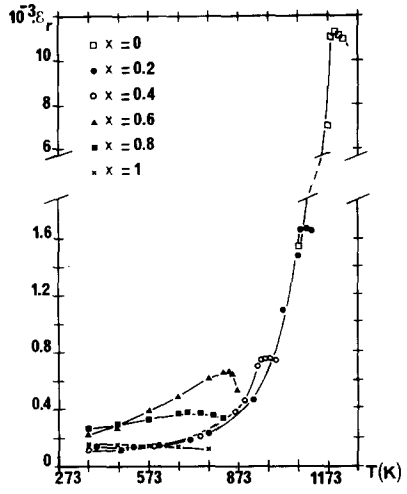

Fig. 13. Evolution of the dielectric constant of $Bi_{3-x}La_xTiNbO_9$ with the lanthanum content x.

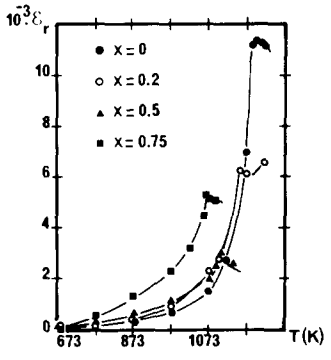

Fig. 14. Evolution of the dielectric constant of $Bi_3Ti_{x/2}Nb_{1-x}W_{x/2}O_9$ with x.

may be used in piezo- or pyroelectric devices working at higher frequency and up to higher temperatures than conventional piezoceramics. For instance, $Bi_4Ti_3O_{12}$-based ceramics are commonly used in accelerometers up to 400 °C.

However, as the spontaneous polarization movements are restricted to the a, b plane (the c axis component can be neglected), the piezoactivity is much lower than for PZT ceramics (Table 4). Conventionally sintered ceramics are difficult to pole because of their very high coercive fields (more than 5 MV m^{-1}).

The trends in layered bismuth oxide materials processing therefore involve mainly:

(i) Single crystal growth for ferroelectric optic devices.

(ii) Grain orientated ceramics, usually obtained by fused salt synthesis, followed by hot forging. The materials are therefore strongly anisotropic; poling is easier in the plane normal to the forging direction, leading to properties highly decoupled along the two perpendicular directions (Fig. 15).

TABLE 4. Typical characteristics of some piezoceramics

	$BaTiO_3$[a]	PZT 1[a]	PZT 2[a]	$Bi_4Ti_3O_{12}$[a]	BPTN[b]	NBT[b]	PBT[b]
T_c (K)[c]	403	603	508	948	618	931	833
ε_r	1900	500	2900	160	106	140	150
$10^4 \tan \delta$[d]	10	30	160	30	–	30	–
k_{33}[e]	0.49	0.62	0.70	0.14	0.14	0.15	0.10
k_{31}[e]	0.21	0.30	0.35	0.06	0.07	0.03	0.04
k_p[e]	0.38	0.50	0.63	0.10	–	–	–
d_{33} (pC N^{-1})[f]	190	160	525	16	13	16	12
d_{33} (pC N^{-1})[f]	−80	−70	−220	−7	−7	−3	−5
Qm[g]	500	2000	90	500	–	–	–
Work range (K)	<373	<503	<423	<723	<523	<723	<673

[a]Commercial materials. [b]BPTN: $Bi_{3.3}Pb_{0.7}Ti_{2.3}Nb_{0.7}O_{12}$; NBT: $Na_{0.5}Bi_{4.5}Ti_4O_{15}$; PBT: $PbBi_4Ti_4O_{15}$ [43, 44].
[c]T_c: Curie temperature. [d]Tan δ: dielectric loss. [e]k: electromechanical coupling factor.
[f]d: piezoelectric strain constant. [g]Q_m: mechanical quality factor.

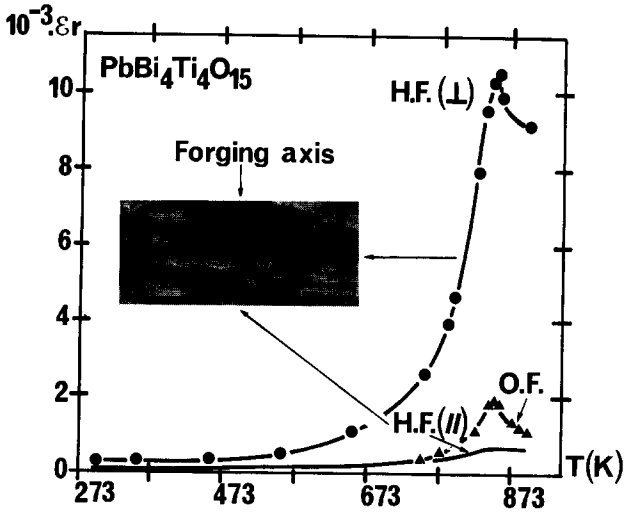

Fig. 15. Temperature dependence of the dielectric constants of $Bi_4PbTi_4O_{15}$ (OF = ordinary forging, HF = hot forging). Insert is an electron micrograph (× 5000) showing the grain orientation.

(iii) Thin films. As it is now possible to deposit thin films directly on the integrated semiconductor driving circuits, the main field of application concerns random access memory devices in which submicron films are needed because polarization switching must be obtained with the low voltage levels (3–5 V) generally used in microelectronics. They can be prepared by techniques such as sputtering, evaporation, chemical vapour deposition, laser ablation and sol–gel deposition. The dielectric properties (remanent polarization, coercive field) and the fatigue or ageing characteristics depend strongly on the microstructure and on the thickness of the film as well as on the nature of the electrodes. Further work is needed to fully optimize the properties of these ferroelectric thin films.

References

1 B. Aurivillius, *Ark. Kemi.*, *1* (1949) 463.
2 B. Aurivillius, *Ark. Kemi.*, *2* (1951) 519.
3 G. A. Smolenskii, V. A. Isupov and A. I. Agranovskaya, *Fiz. Tverd. Tela, Leningrad*, *3* (1961) 895.
4 E. C. Subbarao, *J. Am. Ceram. Soc.*, *45* (1962) 166.
5 E. C. Subbarao, *J. Phys. Chem. Solids*, *23* (1962) 665.
6 R. W. Wolfe and R. E. Newnham, *Solid State Commun.*, *7* (1969) 1797.
7 J. Zemann, *Heidelb. Beitr. Mineral. Petrogr.*, *5* (1956) 139.
8 B. Frit et M. Jaymes, *Bull. Soc. Chim. Fr.*, *3–4* (1974) 402.
9 B. Aurivillius, *Ark. Kemi.*, *5* (1952) 39.
10 I. G. Ismailzade, *Izv. Akad. Nauk SSSR*, *24* (1960) 1198.
11 R. W. Wolfe and R. E. Newnham, *J. Electrochem. Soc.*, *116* (1969) 832.
12 R. E. Newnham, R. W. Wolfe and J. F. Dorrian, *Mater. Res. Bull.*, *6* (1971) 1029.
13 T. Kikuchi, *Mater. Res. Bull.*, *14* (1979) 1561.
14 F. A. Mirishli and I. H. Ismailzade, *Izv. Akad. Nauk SSSR, Ser. Fiz.*, *33* (1967) 91833.
15 G. D. Sultanov, F. A. Mirishli and I. H. Ismailzade, *Ferroelectrics*, *5* (1973) 197.
16 I. H. Ismailzade, V. I. Nesterenko, F. A. Mirishli and P. G. Rustamov, *Kristallografiya*, *12* (1967) 468.
17 I. H. Ismailzade and F. A. Mirishli, *Izv. Akad. Nauk SSSR, Ser. Fiz.*, *33* (1969) 1138.
18 J. L. Hutchinson, J. S. Anderson and C. N. R. Rao, *Proc. R. Soc. London, Ser. A*, *335* (1977) 301.
19 R. W. Wolfe, R. E. Newnham and K. D. Smith, *Ferroelectrics*, *3* (1971) 1.
20 J. F. Dorrian, R. E. Newnham and K. D. Smith, *Ferroelectrics*, *3* (1971) 17.
21 A. D. Rae, J. G. Thompson, R. L. Withers and A. C. Willis, *Acta Crystallogr., Sect. B*, *46* (1990) 474.
22 J. G. Thompson, A. D. Rae, R. L. Withers and D. C. Craig, *Acta Crystallogr., Sect. B*, *47* (1991) 174.
23 A. D. Rae, J. G. Thompson and R. L. Withers, *Acta Crystallogr., Sect. B*, *47* (1991) 870.
24 J. P. Mercurio, A. Souirti, M. Manier and B. Frit, *Mater. Res. Bull.*, *27* (1991) 123.
25 I. G. Ismailzade, *J. Phys. C2*, *33* (2) (1972) 238.

26 R. A. Armstrong and R. E. Newnham, *Mater. Res. Bull.*, *7* (1972) 1025.
27 A. Watanabe, Y. Sekikawa and F. Izumi, *J. Solid State Chem.*, *41* (1982) 138.
28 H. Kodama, F. Izumi and A. Watanabe, *J. Solid State Chem.*, *36* (1981) 349.
29 H. Kodama and A. Watanabe, *J. Solid State Chem.*, *44* (1982) 169.
30 S. Horiuchi, K. Muramatsu and M. Shimazu, *J. Solid State Chem.*, *34* (1980) 51.
31 K. Muramatsu, M. Shimazu, J. Tanaka and S. Horiuchi, *J. Solid State Chem.*, *36* (1981) 179.
32 T. Kikuchi, A. Watanabe and K. Uchida, *Mater. Res. Bull.*, *12* (1977) 299.
33 J. Gopalakrishnan, A. Ramanan, C. N. R. Rav, D. A. Jefferson and D. J. Smith, *J. Solid State Chem.*, *55* (1984) 101.
34 V. I. Voronkova and V. K. Yanovskii, *Phys. Status Solidi*, *101* (1987) 45.
35 S. Horiuchi, T. Kikuchi and M. Goto, *Acta Crystallogr., Sect. A*, *33* (1977) 701.
36 T. Kikuchi, *J. Less-Common Met.*, *52* (1977) 163.
37 G. N. Subbanna, T. N. Guro Row and C. N. R. Rao, *J. Solid State Chem.*, *86* (1990) 206.
38 D. A. Jefferson, M. K. Uppal, C. N. R. Rao and D. J. Smith, *Mater. Res. Bull.*, *19* (1984) 1403.
39 R. L. Withers, J. G. Thompson and A. D. Rae, *J. Solid State Chem.*, *94* (1991) 404.
40 S. E. Cumminus and L. E. Cross, *J. Appl. Phys.*, *39* (5) (1968) 2268.
41 G. A. Smolenskii, V. A. Bokov, V. A. Isupov, N. N. Krainik, R. E. Posynkov and A. I. Sokolov, in G. A. Smolenskin (ed.), *Ferroelectrics and Related Materials*, Gordon and Breach, NY, 1984, p. 696.
42 J. P. Mercurio and B. Frit, *Silic. Ind.*, *9–10* (1989) 143.
43 T. Takenaka and K. Sakata, *J. Appl. Phys.*, *55* (4) (1984) 1092.
44 T. Takenaka and K. Sakata, *Sensors Mater.*, *1* (1988) 35.